Doolittle, R. F. (1984) *Annu. Rev. Biochem. 53*, 195–229.
Engvall, E., & Ruoslahti, E. (1977) *Int. J. Cancer 20*, 1–5.
Folk, J. E., & Finlayson, J. S. (1977) *Adv. Protein Chem. 31*, 1–133.
Freyssinet, J. M., Torbet, J., Hudry-Clergeon, G., & Maret, G. (1983) *Proc. Natl. Acad. Sci. U.S.A. 80*, 1616–1620.
Furie, B. C., & Furie, B. (1976) *Methods Enzymol. 45*, 191–205.
Ganguly, P., Chelladurai, M., Fossett, N., & Jefferson, W. (1983) *Biochem. Biophys. Res. Commun. 116*, 189–194.
Garman, A. J., & Smith, R. A. G. (1982) *Thromb. Res. 27*, 311–320.
Gormsen, J., Fletcher, A. P., Alkjaersing, N., & Sherry, S. (1967) *Arch. Biochem. Biophys. 120*, 654–665.
Greenberg, C. S., & Shuman, M. A. (1982) *J. Biol. Chem. 257*, 6096–6101.
Hantgan, R. R., & Hermans, J. (1979) *J. Biol. Chem. 254*, 11272–11281.
Hermans, J., & McDonagh, J. (1982) *Semin. Thromb. Hemostasis 8*, 11–24.
Hewat, E. A., Tranqui, L., & Wade, R. H. (1983) *J. Mol. Biol. 170*, 203–222.
Jackson, C. M., & Nemerson, Y. (1980) *Annu. Rev. Biochem. 49*, 765–811.
Janus, T. J., Lewis, S. D., Lorand, L., & Shafer, J. A. (1983) *Biochemistry 22*, 6269–6272.
Kekwick, R. A., Mackay, M. E., Nance, M. M., & Record, B. H. (1955) *Biochem. J. 60*, 671–683.
Lorand, L., & Jacobsen, A. (1962) *Nature (London) 195*, 911–912.
Maret, G., & Weill, G. (1983) *Biopolymers 22*, 2727–2744.
Messmore, H. L. (1982) *Semin. Thromb. Hemostasis 8*, 267–275.
Minton, A. P. (1981) *Biopolymers 20*, 2093–2120.
Minton, A. P. (1983) *Mol. Cell. Biochem. 55*, 119–140.
Mosher, D. F. (1976) *J. Biol. Chem. 251*, 1639–1645.
Müller, M. F., Ris, H., & Ferry, J. D. (1984) *J. Mol. Biol. 174*, 369–384.
Nemerson, Y., & Furie, B. (1980) *CRC Crit. Rev. Biochem. 9*, 45–85.
Rakoczi, I., Wiman, B., & Collen, D. (1978) *Biochim. Biophys. Acta 540*, 295–300.
Sakata, Y., & Aoki, N. (1980) *J. Clin. Invest. 65*, 290–297.
Sakata, Y., Mimuro, J., & Aoki, N. (1984) *Blood 63*, 1393–1401.
Shah, G. A., Ferguson, I. A., Dhall, T. Z., & Dhall, D. P. (1982) *Biopolymers 21*, 1037–1047.
Tamaki, T., & Aoki, N. (1981) *Biochim. Biophys. Acta 661*, 280–286.
Torbet, J. (1986) *Biophysical Uses of Steady Magnetic Fields* (Maret, G., Kiepenheuer, J., & Boccara, N., Eds.) Springer-Verlag, New York and Berlin.
Torbet, J., Freyssinet, J. M., & Hudry-Clergeon, G. (1981) *Nature (London) 289*, 91–93.
Wilf, J., Gladner, J. A., & Minton, A. P. (1985) *Thromb. Res. 37*, 681–688.

# Crystal Structure of Substrate-Free *Pseudomonas putida* Cytochrome P-450†

Thomas L. Poulos,* Barry C. Finzel, and Andrew J. Howard
*Protein Engineering Department, Genex Corporation, 16020 Industrial Drive, Gaithersburg, Maryland 20877*
*Received February 27, 1986; Revised Manuscript Received April 30, 1986*

ABSTRACT: The crystal structure of *Pseudomonas putida* cytochrome P-450$_{cam}$ in the substrate-free form has been refined at 2.20-Å resolution and compared to the substrate-bound form of the enzyme. In the absence of the substrate camphor, the P-450$_{cam}$ heme iron atom is hexacoordinate with the sulfur atom of Cys-357 providing one axial heme ligand and a water molecule or hydroxide ion providing the other axial ligand. A network of hydrogen-bonded solvent molecules occupies the substrate pocket in addition to the iron-linked aqua ligand. When a camphor molecule binds, the active site waters including the aqua ligand are displaced, resulting in a pentacoordinate high-spin heme iron atom. Analysis of the $F_{\text{no camphor}} - F_{\text{camphor}}$ difference Fourier and a quantitative comparison of the two refined structures reveal that no detectable conformational change results from camphor binding other than a small repositioning of a phenylalanine side chain that contacts the camphor molecule. However, large decreases in the mean temperature factors of three separate segments of the protein centered on Tyr-96, Thr-185, and Asp-251 result from camphor binding. This indicates that camphor binding decreases the flexibility in these three regions of the P-450$_{cam}$ molecule without altering the mean position of the atoms involved.

Cytochromes P-450 are a group of *b*-type heme proteins that catalyze the hydroxylation of aromatic or aliphatic substrates in a variety of metabolic processes of both prokaryotes and eukaryotes. While a large number of P-450s have been purified and characterized, the cytochrome P-450 camphor 5-exohydroxylase (P-450$_{cam}$) from the soil bacterium *Pseudomonas putida* has provided the most detailed structural and mechanistic information on P-450 monooxygenases (Wagner & Gunsalus, 1982; Gunsalus et al., 1980; Debrunner et al., 1978; Gunsalus & Sligar, 1978).

P-450$_{cam}$ is a 45 000-dalton polypeptide chain containing a single ferric protoporphyrin IX. An abbreviated catalytic cycle for P-450$_{cam}$ is depicted in Scheme I. As in other *b*-type heme proteins, the ferric ($Fe^{3+}$) iron atom in P-450$_{cam}$ equilibrates between the low-spin state, $S = {}^1/_2$, and the high-spin state, $S = {}^5/_2$ (Sharrock et al., 1976; Tsai et al., 1970). As depicted in Scheme I, the low-spin state is favored in the absence of substrate, and the iron atom is hexacoordinate with X representing an unidentified axial ligand. In the presence of

† This work was supported in part by NIH Grants GM 33325 and GM 33688.

0006-2960/86/0425-5314$01.50/0 

substrate, camphor, the spin equilibrium shifts toward the high-spin form (Philson, 1976; Sligar, 1976), and the ligand, X, is displaced. In addition to the substrate-induced shift in spin equilibrium, an increase in the midpoint potential from about −300 to about −173 mV accompanies the change from the low- to high-spin configuration (Sligar & Gunsalus, 1976). This shift in redox potential has mechanistic significance. The physiological reductant of P-450$_{cam}$, the ferredoxin-like iron-sulfur protein putidaredoxin, exhibits a redox potential near −196 mV so that reduction of ferric high-spin P-450$_{cam}$ with substrate bound (−173 mV) is thermodynamically favorable while reduction of ferric low-spin (−300 mV) P-450$_{cam}$ is not (Sligar & Murray, 1986; Sligar & Gunsalus, 1976).

Scheme I

$$\underset{\text{low-spin}}{S^-—Fe^{3+}—X} \overset{R}{\rightleftharpoons} \underset{\text{high-spin}}{S^-—Fe^{3+}R} \xrightarrow{O_2,\ 2e^-}$$

substrate-free substrate-bound

$$S^-—Fe^{3+}—X + R—OH + H_2O$$

Detailed thermodynamic state diagrams elegently categorize the energetics of spin equilibria, redox potential shift, and substrate binding (Sligar & Murray, 1986; Sligar & Gunsalus, 1979; Sligar, 1976). Nevertheless, little is known about the structural details associated with the interconversion of these various forms of P-450$_{cam}$. On the basis of a 2.6-Å crystal structure, we have shown that the high-spin, camphor-bound form of the enzyme involves a pentacoordinate iron atom with only one axial ligand, the sulfur atom of Cys-357 (Poulos et al., 1985). Unknown, however, is the precise identity of the other axial ligand in the low-spin, substrate-free state. Various spectral probes indicate that a sixth axial ligand (X in Scheme I) may be an oxygen atom (Dawson et al., 1982; Philson et al., 1979; Griffin & Peterson, 1975), but whether the oxygen is a component of an amino acid side chain or a solvent molecule remains unclear. In this paper, we present crystallographic data from the substrate-free form of the enzyme and focus on the differences between crystal structures of P-450$_{cam}$ with and without substrate bound.

## Materials and Methods

P-450$_{cam}$ was crystallized according to our earlier procedure (Poulos et al., 1982). These crystals grow in the absence of camphor but with a large excess of dithiothreitol. Dithiothreitol competes with camphor in binding to the enzyme and generates electron paramagnetic resonance and absorption spectra distinct from those of the thiol-free enzymes (Sono et al., 1982). Therefore, crystals were converted to the low-spin, thiol-free form by washing extensively with 0.05 M potassium phosphate, pH 7.0, 40% ammonium sulfate, and 0.2 M KCl.

Removal of dithiothreitol appeared to depend on soak time. Crystallographic refinement with data obtained from crystals soaked for only 12–24 h indicated residual-bound dithiothreitol at relatively high occupancy (~>60%). This was evidenced by low-temperature factors and positive $F_o - F_c$ difference density at scattering centers initially modeled as solvent oxygen atoms. A model that best accounted for $F_o - F_c$ difference density included a cluster of active site water molecules and a dithiothreitol molecule, each at about half-occupancy. Crystallographic refinement with data obtained from a single crystal washed every other day over a 2-week period gave no evidence of ordered high-occupancy sulfur atoms in the substrate pocket. Furthermore, single-crystal EPR (Devaney, 1980; Devaney et al., 1980) and single-crystal polarized absorption spectroscopy (Gerald C. Wagner, personal communication) with crystals grown and then washed in thiol-free mother liquor exactly as described here generated spectra indistinguishable from those of solutions of ferric, low-spin, substrate-free P-450$_{cam}$ with no indication of bound dithiothreitol. The data we report here were obtained from a single crystal soaked over the 2-week period.

Diffraction data were obtained from a single crystal to 2.2-Å resolution with a Xentronics area detector and a rotating anode X-ray source (70 mA, 40 kV) equipped with a graphite monochromator. Details of data collection will be described elsewhere (Howard et al., 1986). The final scaling $R_{merge}$ for 122 589 observations of 18 439 unique reflections to a maximum resolution of 2.20 Å (85% of the total possible) was 0.068, where

$$R_{merge} = \sum|I_i - \langle I_i\rangle|/\sum I_i$$

and $I_i$ is the intensity of the $i$th observation and $\langle I_i\rangle$ is the mean intensity of that reflection. Of the 18 439 unique reflections to 2.2 Å, 16 239 have $\langle I\rangle \geq \sigma_I$. In reduction of the data to obtain scaled structure factors, Friedel mates were merged.

Background levels for difference Fouriers were taken to be $\sigma$, the root mean square difference density computed over an asymmetric unit. Electron density maps were examined and models constructued by using an Evans and Sutherland PS300 color system supporting FRODO (Jones, 1978). Crystallographic refinement was carried out with the restrained parameters least-squares refinement of Hendrickson and Konnert (1980).

## Results and Discussion

*P-450$_{cam}$ Structure.* Since publication of the 2.6-Å crystal structure of the high-spin, camphor-bound form of P-450$_{cam}$ (Poulos et al., 1985), we have extended diffraction data to 1.6 Å and refined the atomic model to an $R$ value of 0.19. Complete details of the refinement and structure of this species will be presented elsewhere (unpublished results). Summary statistics for refinement of the camphor-bound structure are presented in Table I. As this model is considerably more accurate than that which resulted from our earlier work, it was used for initial comparison against data from the camphor-free form.

Figure 1 shows the overall topography of the P-450$_{cam}$ structure, and Figure 2A depicts the active site environment. Deeply embedded in the protein, the camphor molecule sits just above the heme directly adjacent to the oxygen binding site. Complementary hydrophobic contacts hold the camphor in place while the only polar contact is a hydrogen bond between the side-chain hydroxyl group of Tyr-96 and the camphor carbonyl oxygen atom. An iron-bound oxygen atom would contact the camphor molecule on the exo surface of carbon 5, giving 5-*exo*-hydroxycamphor, the only product found in the completely reconstituted P-450$_{cam}$ monooxygenase system (Gelb et al., 1982).

*$F_{\text{no camphor}} - F_{\text{camphor}}$ Difference Fourier.* To begin a comparison of the camphor-bound vs. camphor-free forms of the enzyme, a $(F_{\text{no camphor}} - F_{\text{camphor}})\alpha_{\text{camphor}}$ difference electron density map was computed and analyzed. Figure 3A shows difference density in the vicinity of the camphor binding pocket. The most prominent feature of the difference map is a spherical lobe of positive difference density with a maximum value of 8$\sigma$ in the axial coordination position. We interpret this difference density as a solvent molecule coordinated with the iron atom. A 3$\sigma$ negative difference density surrounds a portion of the volume formerly occupied by the camphor molecule. Because the negative difference density does not envelop the entire substrate molecule, other scattering material must have substituted for the camphor molecule.

FIGURE 1: A stereochemical $\alpha$-carbon backbone model of refined 1.6-Å P-450$_{cam}$ model. Both the camphor and the heme are shown. The $\alpha$-carbon position of every 30 residues is labeled.

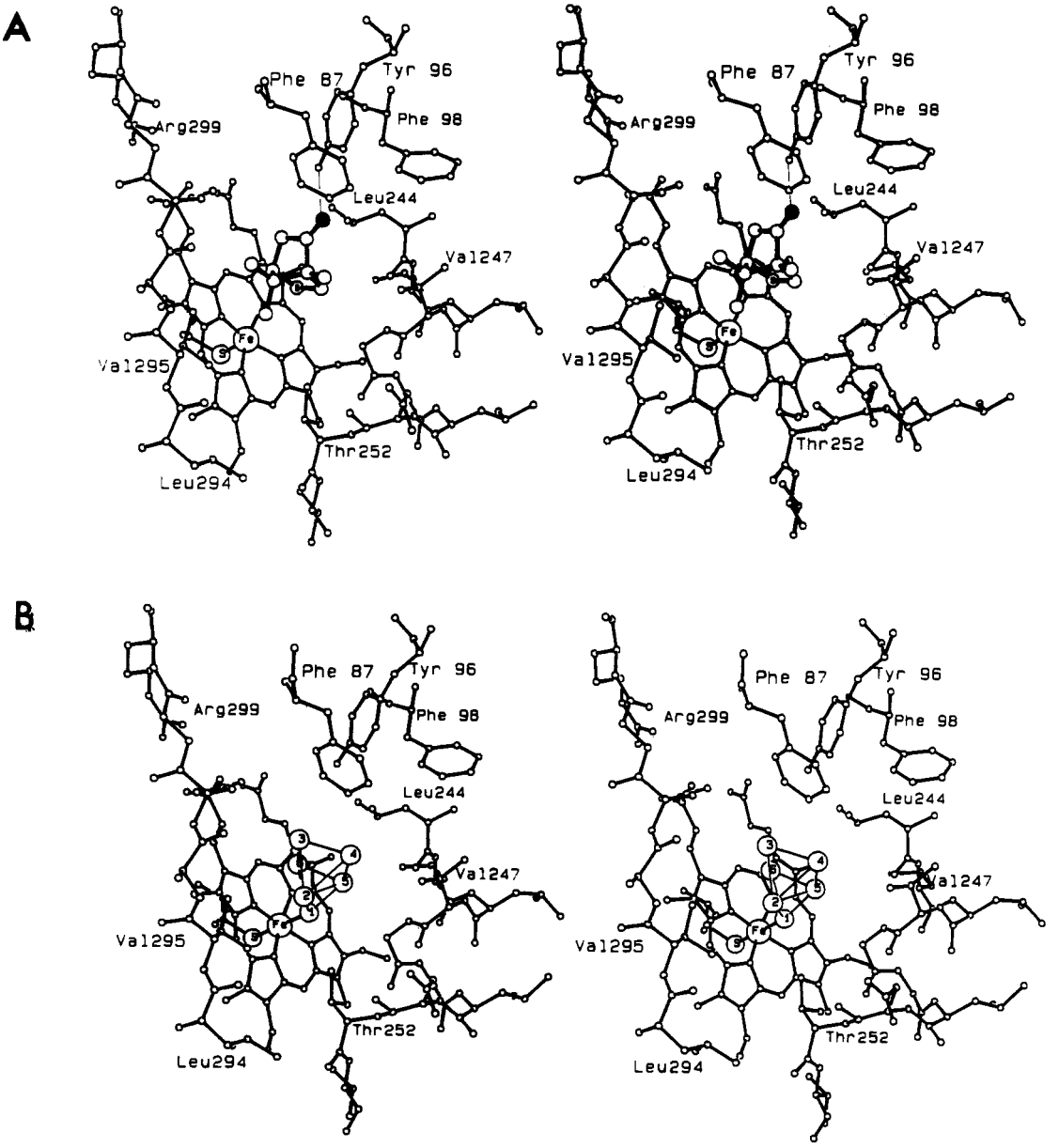


FIGURE 2: Stereochemical models of active site environment in P-450$_{cam}$. (A) The camphor-bound form of the enzyme showing the camphor in place with carbon 5 labeled. The dark atom indicates the camphor carbonyl oxygen atom. (B) The substrate-free form of the enzyme showing the active site solvent structure. The solvent molecules are labeled in the order with which they were added to the model during the course of refinement. Thin lines in both diagrams indicate hydrogen bonds.

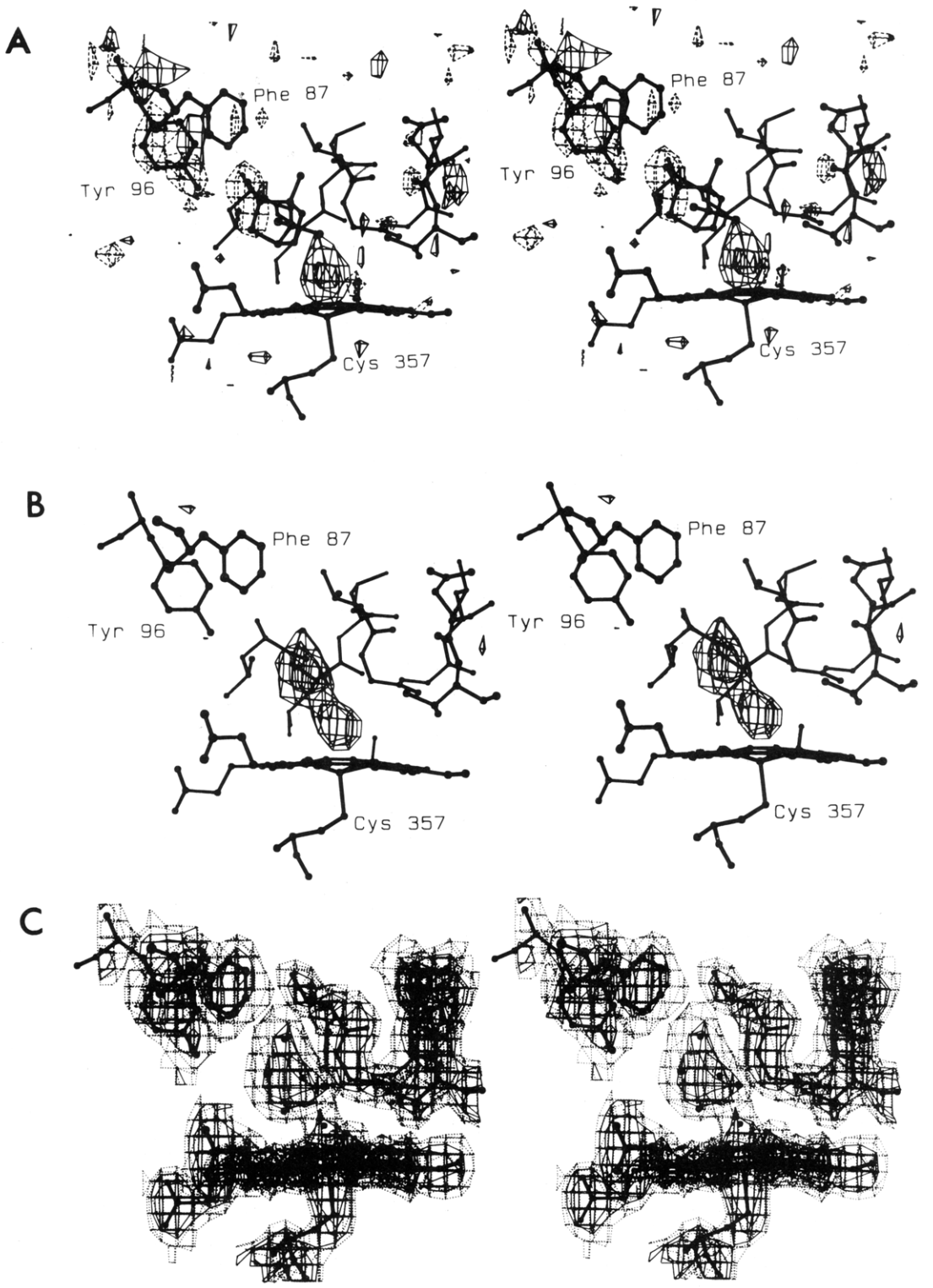


FIGURE 3: Electron density difference maps in vicinity of active site. $\sigma$ is the root mean square difference density computed over an entire asymmetric unit. (A) The $(F_{\text{no camphor}} - F_{\text{camphor}})\alpha_{\text{camphor}}$ difference electron density map contoured at $\pm 3\sigma$ and $\pm 7\sigma$. In both (A) and (B), positive contours are indicated by solid lines and negative contours by dashed lines. (B) The first $(F_0 - F_c)\alpha_{\text{camphor}}$ difference electron density map obtained after four cycles of restrained parameters least-squares refinement against the camphor-free data. Positive contours are shown at $+4\sigma$ and $+5\sigma$. There are no negative contours at these levels. (C) The final $2F_0 - F_c$ electron density map. Two contour levels are shown to indicate that the iron-linked aqua ligand is resolved from the active site solvent molecules at higher contour levels.

Because we detected no movement of protein groups into the camphor pocket, we have concluded that solvent molecules occupy the active site pocket in the absence of camphor. The only side chains that undergo significant perturbations are those of Phe-87 and Tyr-96, both of which contact the camphor molecule (Figure 2A). A $3\sigma$ negative difference density surrounds Tyr-96 and, to a lesser extent, Phe-87. Negative difference density more fully surrounds Phe-87 at the $2\sigma$ level. A $3\sigma$ positive peak is situated between the phenyl and tyrosyl rings. Because only one positive difference peak is associated with both Phe-87 and Tyr-96, it was not possible to determine precisely how the aromatic rings should be repositioned from the difference Fourier alone. As we will discuss further on when we consider temperature factor changes, the positive difference density corresponds to movement of Phe-87 while the negative difference density surrounding Tyr-96 results from

Table I: Summary of Least-Squares Refinement Parameters and Geometric Conformity

| | Least-Squares Refinement | |
|---|---|---|
| | camphor bound | camphor free |
| cell parameters, $a$, $b$, $c$ (Å) | 108.67, 103.80, 36.38 | 108.46, 104.21, 36.11 |
| space group $P2_12_12_1$ | | |
| nominal resolution (Å) | 10 → 1.61 | 10 → 2.20 |
| reflections | | |
| measured | 42 513 | 18 983 |
| used ($I \geq \sigma_I$) | 34 551 | 16 395 |
| $R = \sum\|F_0 - F_c\|/\sum F_0$ | 0.193 | 0.176 |
| | Geometric Conformity[a] | |
| | camphor bound | camphor free |
| distances | | |
| 1–2 | 0.024 | 0.016 |
| 1–3 | 0.034 | 0.030 |
| 1–4 | 0.039 | 0.031 |
| planes | | |
| peptides | 0.029 | 0.024 |
| other | 0.012 | 0.009 |
| chiral volumes | 0.264 | 0.240 |
| nonbonded contacts | | |
| 1–4 | 0.180 | 0.175 |
| other | 0.121 | 0.135 |
| thermal parameter correlations | | |
| main-chain 1–2 | 0.943 | 0.664 |
| main-chain 1–3 | 1.399 | 1.116 |
| side-chain 1–2 | 1.928 | 1.310 |
| side-chain 1–3 | 2.825 | 2.064 |

[a] Values are the root mean square deviations (Å) from expected geometry following restrained-parameter least-squares refinement. Thermal parameter values relate mean difference in isotropic temperature factor (Å$^2$) between pairs of atoms. The notations 1–2, 1–3, and 1–4 refer to atom pairs related through a bond, a bond angle, or a dihedral angle, respectively.

increased thermal motion of the tyrosyl side chain.

*Refinement of Camphor-Free Structure.* A more reliable method for determining changes between the camphor-bound and -free forms of the enzyme is to refine each structure separately, relying on $F_0 - F_c$ difference Fouriers and then compare the two refined structures. To refine the camphor-free structure, we started with the refined camphor-bound structure, removed the camphor molecule, and subjected the camphor-free model to several rounds of restrained least-squares refinement against the camphor-free data. At this stage, we made no attempt to model the active site solvent structure. After four cycles of refinement the $R$ factor to 2.2 Å was 0.193. Figure 3B shows the resulting $(F_0 - F_c)\ \alpha_{\text{no camphor}}$ electron density map and more clearly demonstrates that the axial coordination position and camphor pocket are occupied by positive density features, which once again represent solvent molecules. The volume of electron density in the camphor pocket readily accommodates five solvent molecules in addition to the iron-linked aqua ligand. A single water molecule was positioned into the $F_0 - F_c$ electron density map in the axial coordination position followed by three more cycles of refinement. A second water molecule was placed in the resulting electron density maps followed by eight cycles of refinement, which lowered $R$ to 0.183. At this stage, the remaining active site solvents were fitted to the electron density maps followed by four more cycles of refinement. Throughout the map-fitting process, only features at the $\pm 3\sigma$ level in difference electron density maps were considered significant. After refinement, the average temperature factor for the five active site water molecules was somewhat higher than that of ordered surface water molecules, 34 Å$^2$ vs. 29 Å$^2$, while the occupanices were comparable, 0.78 vs. 0.90. However, surface water temperature factors ranged from as low as 6 Å$^2$ up to 50 Å$^2$ while the active site waters all clustered near the average. The iron-linked aqua ligand exhibited a temperature factor of 16.5 Å$^2$ with an occupancy of 1.0. The Fe–O bond distance obtained from the final refined model is 2.28 Å. Figure 3C shows the final $2F_0 - F_c$ map.

While inclusion of this solvent model eliminated nearly all significant difference density in the vicinity of the active site, only the iron-linked aqua ligand has been resolved as an isolated sphere of electron density (Figure 3C). The remaining five solvent molecules in the substrate pocket occupy a large lobe of unresolved electron density as exemplified by the first $F_0 - F_c$ electron density map (Figure 3B,C). In modeling the active site solvent structure, we attempted to place solvent in positions of maximum difference electron density while simultaneously optimizing potential hydrogen-bonding interactions between molecules. The resulting interconnected cluster (Figure 2B) fulfills reasonable packing restrictions, but probably represents only one of many energetically similar configurations that coexist. Such microheterogeneity would account for our failure to resolve individual solvent peaks and may be observed because of an absence of hydrophilic protein groups in the active site capable of inducing a strong preference to any particular configuration.

Alternatively, we have considered the possibility that our inability to resolve the active site water molecules is due to the partial occupancy of another large solvent ion. Sulfate is a plausible candidate because the crystals are stored in 40% ammonium sulfate. A sulfate ion hydrogen bonded to the aqua ligand accounts for the electron density nearly as well as the water cluster model. Moreover, the final $F_0 - F_c$ electron density map phased with the water cluster model exhibited a small positive $4\sigma$ peak near the center of the water cluster, possibly due to a sulfur atom at fractional occupancy. Therefore, we refined the structure using the sulfate–aqua ligand model. Temperature factors for the sulfate atoms were held constant at the mean value for all atoms in the structure, 21 Å$^2$, and only occupancies were allowed to vary. After four cycles of refinement, occupancies for the sulfate atoms converged to the following values: O1 = 0.77, O2 = 0.58, O3 = 0.65, O4 = 0.57, and S = 0.34. From these data one cannot provide a very convincing argument that sulfate is present even at fractional occupancy. The $4\sigma$ $F_0 - F_c$ peak at the center of the water cluster could also have resulted from yet another water molecule. One additional argument against a sulfate ion is that introduction of two additional negative charges at the active site would be energetically unfavorable without stabilization by hydrogen bonds or a counterion. Thus, the partially ordered five-water cluster remains the best model.

Because the initial $F_{\text{no camphor}} - F_{\text{camphor}}$ electron density difference map indicated movement of Tyr-96, Phe-87, and possibly residues 94 and 95, an "omit" map was computed with these residues excluded from the structure factor calculation. After refitting these residues to $F_0 - F_c$ and $2F_0 - F_c$ electron density maps, several cycles of refinement were carried out until $R$ converged to a value of 0.176. Final refinement statistics are listed in Table I.

*Comparison of the Two Structures.* To quantify differences between the camphor-free and -bound structures, we first superimposed the two structures and optimized the fit between common protein and heme atoms using a least-squares procedure. The resulting root mean square fit between main-chain atoms was 0.17 Å and between side chains 0.23 Å. Several side chains exhibited shifts equal to or greater than the root mean square value, but most of these were surface residues exhibiting high temperature factors in both structures. Of the

two active site residues, Phe-87 and Tyr-96, whose movement was indicated by the $F_{\text{no camphor}} - F_{\text{camphor}}$ difference Fourier, only Phe-87 underwent a significant shift. The phenyl ring moves about 0.3 Å in toward the camphor pocket in the camphor-free structure, presumably to occupy part of the volume vacated by the substrate molecule. The only change in Tyr-96 was an increase in mean temperature factor from 14 Å$^2$ in the camphor structure to 32 Å$^2$ in the camphor-free structure. Thus, negative difference density surrounding Tyr-96 was the result of increased thermal motion of the Tyr-96 side chain.

The Tyr-96–camphor hydrogen bond (Figure 2A) is not replaced with a Tyr-96-ordered water molecule hydrogen bond. Water 3 (Figure 2b) is closest to Tyr-96 but is too far (~4 Å) from the Tyr-96 hydroxyl group for hydrogen-bonding interactions.

Perturbation of a single tyrosine residue upon substrate binding also is indicated from camphor-induced UV spectral changes (Fisher & Sligar, 1985). The tyrosine in question is very likely Tyr-96. In the absence of camphor, both Tyr-96 and the heme experience a polar environment due to the surrounding active site water molecules. When camphor binds, the Tyr-96 environment becomes nonpolar, resulting in the observed UV spectral shift even though Tyr-96 does not undergo a conformational change detectable in our 2.2-Å maps. Here is an example of where one must exercise caution in interpreting UV spectral changes. Aromatic amino acid difference spectra usually are associated with conformational changes. With P-450$_{cam}$, however, only the dielectric environment surrounding Tyr-96 changes, not the position of the aromatic ring.

In the camphor-free structure, the iron atom is displaced about 0.30 Å from the porphyrin core, while this displacement is 0.44 Å in the camphor-bound structure, suggesting that the iron atom moves about 0.14 Å toward Cys-357 in the low- to high-spin transition. To assess whether or not a 0.14-Å difference is significant requires a method for estimating the error in measuring the displacement of the iron atom from the heme plane. Two procedures commonly are used in protein crystallography to estimate errors in atomic coordinates (Cruickshank, 1967, 1954; Luzzati, 1952; Cruickshank, 1949). From the method of Luzzati, the estimated overall root mean square error for the camphor-free structure is 0.21 Å while the Cruickshank method gives 0.24 Å. One advantage of the Cruickshank method is that atom type and temperature factor are taken into account. On the basis of this procedure, the error in determining the position of the iron atom in the camphor-free structure is only 0.03 Å while that of the pyrrole ring nitrogens is 0.14 Å. Thus, the apparent motion of the iron atom relative to the porphyrin core is just on the verge of being significant. Furthermore, if displacement of the iron atom had changed to the extent that it does in the deoxy to carbonmonoxy hemoglobin transition (Baldwin & Chothia, 1979), the $F_{\text{no camphor}} - F_{\text{camphor}}$ difference Fourier would have shown some difference density around the porphyrin core, which it did not. As a result, we must conlude that we are unable to detect significant differences in the displacement of the iron atom from the porphyrin core.

*Comparison of Temperature Factors.* Crystallographic Debye–Waller "temperature" or "*B*" factors are related to atomic root mean square vibration amplitudes and are determined for each protein atom by crystallographic refinement techniques. In some cases, *B* factors appear to correlate well with functionally important dynamical motions of proteins (Karplus & McCammon, 1983; van Gunsteren & Karplus, 1981). Unfortunately, *B* factors also incorporate local disorder and crystalline lattice effects (Finzel & Salemme, 1985; Frauenfelder et al., 1979), which complicate the direct extraction of dynamical information from these parameters. In this comparison, data sets were obtained from two isomorphous crystal forms that differ only by the presence or absence of a substrate molecule. Both the camphor-free and camphor-bound data sets were collected at ambient temperature, and the overall mean temperature factors obtained from refinement of each are comparable: 21.9 Å$^2$ for the camphor-free data and 18.8 Å$^2$ for the camphor-bound data. Additionally, crystals were approximately of the same size and mosaicity. Furthermore, because differences between *B* factors for corresponding atoms in the two structures are generally small, it is reasonable to assert that protein molecules in the two states are subject to nearly identical pressures from their crystalline environments. Any statistically meaningful difference in temperature factors can probably be directly related to differences in dynamical properties of the molecules.

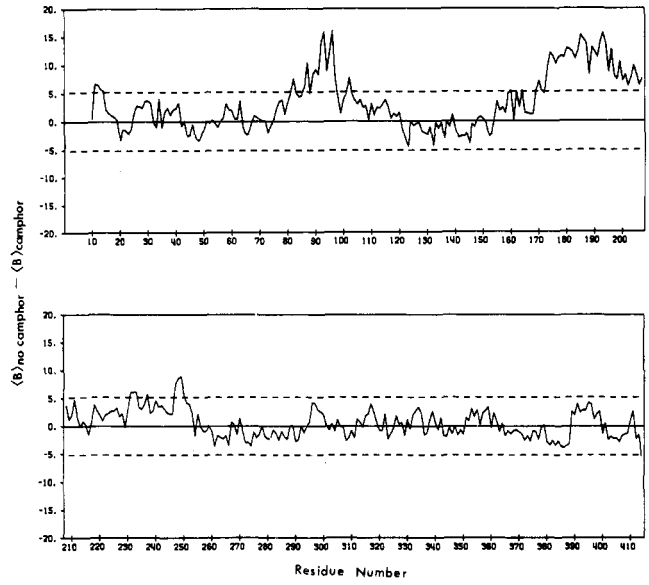


FIGURE 4: Plot of difference in mean temperature factor between camphor-free and camphor-bound (no camphor – camphor) structures as a function of residue number. The dashed lines indicate the root mean square difference in mean temperature factors, which is 5.2 Å$^2$.

To analyze differences in *B* factors between the two forms of P-450$_{cam}$, we first computed the mean *B* factor for each residue in each structure. Then, the difference in mean *B* factor between the camphor-free and -bound structures was plotted as a function of residue number (Figure 4). As shown in Figure 4, there are three regions in the P-450$_{cam}$ molecule centered on Tyr-96, Thr-185, and Asp-251 where larger temperature factors in the camphor-free structure gave rise to differences well above the root mean square difference in mean *B*'s. Tyr-96 and Phe-87, of course, directly contact the camphor molecule (Figure 2A). It therefore appears that the binding of camphor decreases the thermal motion of residues 87–96 owing to formation of the Tyr-96–camphor hydrogen bond and the resulting hydrophobic contact between Phe-87 and the camphor molecule (Figure 2A). A somewhat more interesting change occurs in the region centered on Thr-185. As shown in Figure 5, residues 184–187 form a loop connecting two antiparallel helices on the molecular surface. At the center of this loop, Thr-185 sits about 4 Å above the camphor molecule where its side-chain methyl group contacts the camphor molecule (Figure 5B). As with Phe-87, Thr-185 experiences a decrease in thermal motion owing to the for-

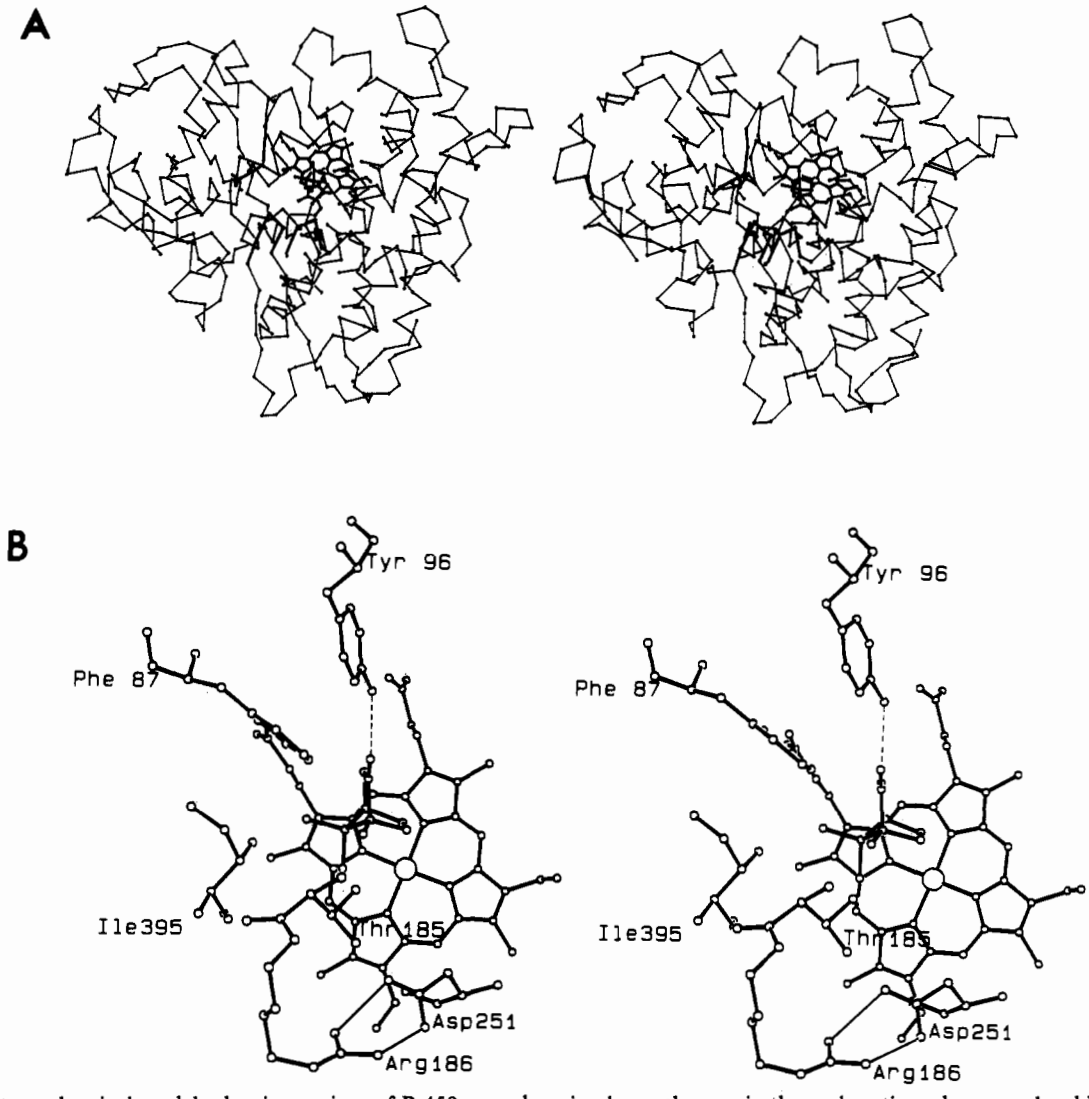


FIGURE 5: Stereochemical models showing regions of P-450$_{cam}$ undergoing large changes in thermal motion when camphor binds. (A) An $\alpha$-carbon backbone model with those segments forming the suspected substrate entrance channel highlighted with thicker bonds. (B) Close-up view of those regions undergoing large shifts in thermal parameters. The-185, Ile-395, Phe-87, and Tyr-96 contact the camphor molecule. The thin lines joining Arg-186 and Asp-251 denote the ion pair. Ile-395 does not undergo as large a change in temperature factor but is shown nonetheless because the surface loop centered on Ile-395 forms part of the small opening above the camphor molecule. Both diagrams are nearly in the same orientation.

mation of hydrophobic contacts with the substrate molecule. Furthermore, the Thr-185 loop together with Phe-87 and Ile-395 form a small opening above the camphor site, which we described earlier as a possible path for the entry of a substrate molecule into the active site (Poulos, 1986; Poulos et al., 1985). Examination of the computed surface of the entire P-450$_{cam}$ structure, however, reveals that a camphor molecule is simply too large to fit into this gap. Thus, enhanced flexibility in this region in the absence of camphor may allow entry of a substrate molecule into the active site.

The last region that undergoes a substrate-induced decrease in thermal motion is near Asp-251. Asp-251 neither contacts the substrate nor forms part of an access channel. Notice, however, that Asp-251 and Arg-186 form an internal ion pair (Figure 5B). Thus, changes in thermal parameters of Asp-251 are coupled to changes in flexibility of the 184–187 loop. Residues contacting the camphor molecule that did not exhibit large changes in thermal parameters include Leu-244, Val-247, Thr-252, and Val-295.

## Conclusions and Summary

Major findings from this study can be summarized as follows. First, a hydroxide ion or water molecule serves as an axial ligand in the low-spin, camphor-free form of the enzyme, and a hydrogen-bonded network of solvent molecules occupies the camphor pocket in the absence of substrate. Earlier results obtained from magnetic resonance techniques also suggest an aqua ligand (Philson et al., 1979; Griffin & Peterson, 1975). Second, no significant differences in the conformation of the polypeptide backbone or side-chain atoms in the camphor-free and -bound structures were found, with the exception of a slight repositioning of Phe-87. Small-angle X-ray scattering data obtained from solutions of P-450$_{cam}$ also demonstrated that the overall size and shape of P-450$_{cam}$ in the substrate-free and -bound forms are indistinguishable (Lewis & Sligar, 1983). Third, substrate binding results in large decreases in thermal motion of at least three segments of P-450$_{cam}$ intimately associated with substrate–protein interactions and, possibly, the substrate-access channel. Thus, local dynamical fluctuations may allow entry of the substrate molecule into the active site, and then, once substrate is bound, flexibility of the entry channel decreases owing to specific protein-substrate interactions.

Availability of refined P-450$_{cam}$ structures in the substrate-free and -bound forms provides a structural basis for

attempting to correlate structural differences with the observed spectral and redox potential shifts that accompany substrate binding. First, we consider the redox potential shift from −300 to −173 mV resulting from substrate binding. In a theoretical treatment of redox potentials in *c*-type cytochromes, Kassner (1972) suggested that differences in the local nonpolar heme environment in various *c*-type cytochromes gives rise to the observed differences in redox potentials. Heme in the ferric, $Fe^{3+}$, state with a net positive charge should be stabilized in a polar environment relative to the ferro heme. Structural comparisons of oxidized and reduced cytochrome *c* (Takano & Dickerson, 1980) and correlations between the cytochrome *c* peroxidase and myoglobin structures with their respective redox potentials support Kassner's hypothesis (Poulos & Finzel, 1984; Conroy et al., 1978; Cassatt et al., 1975). Thus in P-450$_{cam}$, displacement of the active site water molecules by the camphor molecule decreases the polarity of the heme environment, thereby shifting the redox equilibrium toward the ferro ($Fe^{2+}$) oxidation state. Furthermore, the camphor molecule, owing to its close proximity to the oxygen binding site, displaces the iron-linked water molecule or hydroxide ion, which also aids in shifting not only the redox potential but the spin equilibrium toward the pentacoordinate, high-spin state. The presence of substrate should also effect the binding properties of other ligands. Certainly this is the case with the cholesterol side-chain cleavage P-450, P-450$_{scc}$, where CO can be more readily displaced when substrate is bound and where CO binding is much slower in the presence of substrate (Mitani et al., 1985). Such results are expected if the steroid substrate molecule sterically crowds the CO axial coordination position as the camphor molecule does in P-450$_{cam}$.

While the above explanations provide some insight into how changes within the heme pocket relate to redox potential shifts, one should not neglect how the protein as a whole responds to shifts in spin and redox equilibria. Such equilibria describe free-energy states of the entire protein, not simply changes in the heme environment. Any explanation of changes in spin and redox equilibria also reflect changes in conformational or dynamical states of the protein. There is no better example than cytochrome *c*, where clearly defined differences in solution properties of the protein are observed between the oxidized and reduced proteins [reviewed by Salemme (1977)]. Yet, the large changes in solution properties remain difficult to correlate with the refined oxidized and reduced X-ray structures (Takano & Dickerson, 1980). Dynamical properties not detectable in static X-ray structures very likely contribute to the observed differences. Therefore, the question we must address in P-450$_{cam}$ is the relationship between substrate binding with its associated redox and spin-state shifts and conformational and dynamical states of the protein as a whole. Part of the answer very likely relates to the increased stability of the substrate-bound form of the enzyme. Jung et al. (1985) determined, using differential scanning calorimetry, that the midpoint in the thermal transition from folded to unfolded P-450$_{cam}$ is 10 °C higher in the presence of camphor and that the melting of P-450$_{cam}$ becomes a more cooperative process with substrate bound. Dynamical fluctuations are more likely the cause for this increase in stability rather than conformationally distinct states because we observed only limited differences in atomic positions between the camphor-free and -bound structures, yet we did find isolated segments that undergo large changes in thermal motion. Moreover, entropic factors drive substrate binding (Griffin & Peterson, 1972) presumably due to the release of active site water molecules identified in this study and to desolvation of the substrate molecule. Thus, the increase in spin state and redox potential upon substrate binding results from stabilization of P-450$_{cam}$ in a form where the active site dielectric environment is low owing to the entropically favored release of solvent molecules and not from large conformational changes. Identification of regions in P-450$_{cam}$ that experience large shifts in thermal motion also points to significant differences in dynamical properties between the substrate-free and -bound forms of P-450$_{cam}$.

## ACKNOWLEDGMENTS

We thank Professor I. C. Gunsalus for the generous gift of P-450$_{cam}$, Dr. Gerald C. Wagner for permission to quote his single-crystal spectral results prior to publication, Drs. David Davies and Steven Sheriff for reminding us about the possibility of sulfate at the active site, and Dr. Gary Gilliland for reviewing the manuscript.

**Registry No.** Cytochrome P-450, 9035-51-2.

## REFERENCES

Baldwin, J., & Chothia, C. (1979) *J. Mol. Biol. 129*, 175–220.

Cassatt, J. C., Marini, C. P., & Bender, J. (1975) *Biochemistry 14*, 5470–5474.

Conroy, C. W., Tyma, P., Daum, P. H., & Erman, J. E. (1978) *Biochim. Biophys. Acta 537*, 62–69.

Cruickshank, D. W. J. (1949) *Acta Crystallogr. 2*, 65–82.

Cruickshank, D. W. J. (1954) *Acta Crystallogr. 7*, 519.

Cruickshank, D. W. J. (1967) in *International Tables for X-Ray Crystallography* (Kasper, J. S., & Lonsdale, K., Eds.) Vol. 2, pp 318–340, Kynoch, Birmingham, AL.

Dawson, J. H., Anderson, L. A., & Sono, M. (1982) *J. Biol. Chem. 257*, 3606–3617.

Debrunner, P. G., Gunsalus, I. C., Sligar, S. G., & Wagner, G. C. (1978) *Met. Biol. Syst. 7*, 241–275.

Devaney, P. W. (1980) Ph.D. Thesis, University of Illinois.

Devaney, P. W., Wagner, G. C., Debrunner, P. G., & Gunsalus, F. C. (1980) *Fed. Proc., Fed. Am. Soc. Exp. Biol. 39*, 1824.

Finzel, B. C., & Salemme, F. R. (1985) *Nature (London) 315*, 686–688.

Finzel, B. C., Poulos, T. L., & Kraut, J. (1984) *J. Biol. Chem. 259*, 13027–13036.

Fisher, M. T., & Sligar, S. G. (1985) *J. Biochem. (Tokyo) 24*, 6896–6701.

Frauenfelder, H., Petsko, G. A., & Tsernoglou, D. (1979) *Nature (London) 280*, 558–563.

Gelb, M. H., Heimbrook, D. C., Malkonen, P., & Sligar, S. G. (1982) *Biochemistry 21*, 370–377.

Griffin, B. W., & Peterson, J. A. (1972) *Biochemistry 11*, 4740–4746.

Griffin, B. W., & Peterson, J. A. (1975) *J. Biol. Chem. 250*, 6445–6451.

Gunsalus, I. C., & Sligar, S. G. (1978) *Adv. Enzymol. Relat. Areas Mol. Biol. 47*, 1–44.

Gunsalus, I. C., Wagner, G. C., & Debrunner, P. G. (1980) in *Microsomes, Drug Oxidations, and Chemical Carcinogenesis* (Coon, M. J., Conney, A. H., Estabrook, R. W., Gelboin, H. V., Gillette, J. R., & O'Brien, P. J., Eds.) pp 233–242, Academic, New York.

Hendrickson, W. A., & Konnert, J. H. (1980) in *Computing in Crystallography* (Diamond, R., Ramaseshan, S., & Venkatesan, K., Eds.) pp 1301–1323, Indian Institute of Science, Bengalore, India.

Howard, A. J., Gilliland, G., Finzel, B. C., Poulos, T. L., Ohlendorf, D. H., & Salemme, F. R. (1986) *J. Appl. Crystallogr.* (submitted for publication).

Jones, T. A. (1978) *J. Appl. Crystallogr. 11*, 268-272.
Jung, C., Bendzko, P., Ristau, O., & Gunsalus, I. C. (1985) in *Cytochrome P450, Biochemistry, Biophysics, and Induction* (Vereczkey, L., & Magyar, K., Eds.) pp 19-22, Akademiai Kiado, Budapest.
Karplus, M., & McCammon, J. A. (1983) *Annu. Rev. Biochem. 53*, 263-300.
Kassner, R. J. (1972) *J. Am. Chem. Soc. 95*, 2674-2677.
Lewis, B. A., & Sligar, S. G. (1983) *J. Biol. Chem. 258*, 3591-3601.
Luzzati, V. (1952) *Acta Crystallogr. 5*, 802-810.
Mitani, F., Tetsutaro, I., Shimada, H., Ueno, R., & Ishimura, Y. (1985) *J. Biol. Chem. 260*, 12042-12048.
Philson, S. B. (1976) Ph.D. Thesis, University of Illinois, Urbana, IL.
Philson, S. B., Debrunner, P. G., Schmidt, P. G., & Gunsalus, I. C. (1979) *J. Biol. Chem. 254*, 10173-10179.
Poulos, T. L. (1986) in *Cytochrome P450: Structure, Mechanism, and Biochemistry* (Ortiz de Montellano, P. R., Ed.) pp 505-523, Plenum, New York.
Poulos, T. L., & Finzel, B. C. (1984) *Pept. Protein Rev. 4*, 115-171.
Poulos, T. L., Perez, M., & Wagner, G. C. (1982) *J. Biol. Chem. 257*, 10427-10429.
Poulos, T. L., Finzel, B. C., Gunsalus, I. C., Wagner, G. C., & Kraut, J. (1985) *J. Biol. Chem. 260*, 16122-16130.
Salemme, F. R. (1977) *Annu. Rev. Biochem. 46*, 299-329.
Sharrock, M., Debrunner, P. G., Schulz, C., Lipscomb, J. D., Marshall, V., & Gunsalus, I. C. (1976) *Biochim. Biophys. Acta 420*, 8-26.
Sligar, S. G. (1976) *Biochemistry 15*, 5399-5406.
Sligar, S. G., & Gunsalus, I. C. (1976) *Proc. Natl. Acad. Sci. U.S.A. 73*, 1078-1082.
Sligar, S. G., & Gunsalus, I. C. (1979) *Biochemistry 18*, 2290-2295.
Sligar, S. G., & Murray, R. I. (1986) in *Cytochrome P450: Structure, Mechanism, and Biochemistry* (Ortiz de Montellano, P. R., Ed.) pp 429-503, Plenum, New York.
Sono, M., Anderson, L. A., & Dawson, J. H. (1982) *J. Biol. Chem. 257*, 8308-8320.
Takano, T., & Dickerson, R. E. (1980) *Proc. Natl. Acad. Sci. U.S.A. 77*, 6371-6375.
Tsai, R., Yu, C. A., Gunsalus, I. C., Peisach, J., Blumberg, W., Orme-Johnson, W. H., & Beinart, H. (1970) *Proc. Natl. Acad. Sci. U.S.A. 66*, 1157-1163.
Van Gunsteren, W. F., & Karplus, M. (1981) *Nature (London) 293*, 677-678.
Wagner, G. C., & Gunsalus, I. E. (1982) in *The Biological Chemistry of Iron* (Dunford, H. B., Dolphin, D., Raymond, K. N., & Sieker, L., Eds.) pp 405-412, Reidel, Boston.

# Chemically Modified Heparins as Inhibitors of Heparan Sulfate Specific Endo-β-glucuronidase (Heparanase) of Metastatic Melanoma Cells†

Tatsuro Irimura, Motowo Nakajima, and Garth L. Nicolson*
*Department of Tumor Biology, The University of Texas M. D. Anderson Hospital and Tumor Institute, Houston, Texas 77030*
*Received February 11, 1986; Revised Manuscript Received April 14, 1986*

ABSTRACT: To determine the significance of the heparan sulfate (HS) degradative endo-β-glucuronidase (heparanase) in tumor invasion and metastasis and to develop possible antimetastatic agents, we synthesized specific inhibitors of this enzyme. We previously found that heparanase activity correlates with the lung colonization abilities of murine B16 melanoma cells and is inhibited by heparin [Nakajima, M., Irimura, T., Di Ferrante, N., & Nicolson, G. L. (1984) *J. Biol. Chem. 259*, 2283-2290]. In this study, heparin was chemically modified in order to determine which portions of its structure are responsible for heparanase inhibitory activity and to obtain heparanase inhibitors that have minimal additional biological effects, such as anticoagulation. *N*-Sulfate groups and *O*-sulfate in heparin were removed separately, and the resultant free amino groups were acetylated or resulfated. Heparin was also reduced at the carboxyl groups of uronic acid. The heparanase inhibitory activities of these heparin derivatives were examined by high-speed gel-permeation chromatography and by the use of radioactive HS immobilized on agarose beads. The results indicated that although *N*-sulfate and *O*-sulfate groups on glucosamine residues, and carboxyl groups on uronic acid residues, are important for heparanase inhibition, they are not essential for full activity. When highly metastatic B16-BL6 melanoma cells were incubated with N-acetylatyed N-desulfated heparin, N-resulfated N- and O-desulfated heparin, or carboxyl-reduced heparin and injected intravenously to syngenic C57BL/6 mice, significant reductions in the numbers of experimental melanoma lung metastases occurred.

The malignancy of solid tumors can be explained, in part, by their abilities to invade and destroy normal tissues, including extracellular matrix and basement membranes (Nicolson, 1982, 1984; Liotta et al., 1983; Irimura et al., 1983b). Glycosaminoglycans, such as heparan sulfate (HS),[1] are important constituents in these structures. Recently, we found that HS degradative activities of murine B16 melanoma sublines correlated with their metastatic lung colonization and invasive

† This study was supported by U.S. Department of Health and Human Services Grants BRSG RR-5511-23 and R01-CA39319 to T.I. and Grant R01-CA42346 to G.L.N. and a grant from the National Foundation for Cancer Research to G.L.N.
* Author to whom correspondence should be addressed.

[1] Abbreviations: DPBS, Dulbecco's phosphate-buffered saline; HS, heparan sulfate; $M_r$, relative molecular weight; Tris-HCl, tris(hydroxymethyl)aminomethane hydrochloride; EDTA, ethylenediaminetetraacetic acid.

0006-2960/86/0425-5322$01.50/0 